Optimal Location and Sizing of PV-UPQC-O in Distribution Feeders with Electric Vehicles Using Gazelle Optimization Algorithm

Ramesh Puppala[1]*   **Chandra Sekhar K[2]**

[1]*Department of Electrical and Electronics Engineering, Dr YSR ANU College of Engineering and Technology, Acharya Nagarjuna University, Guntur -522510, Andhra Pradesh, India*
[2]*R.V.R & J.C. College of Engineering, Chowdavaram, Guntur, Andhra Pradesh, India*
* Corresponding author's Email: ramesh.anucet.eee@gmail.com

Abstract: Renewable energy systems (RESs) and electric vehicles (EVs) are critical components of current power systems for lowering greenhouse gas (GHG) emissions, combating climate change, and providing alternative energy sources. However, high initial costs and a lack of infrastructure, power storage, and power quality (PQ) are potential concerns for RESs and EVs in power systems. Among the numerous power quality (PQ) devices, the unified power quality conditioner (UPQC) can compensate for voltage and current-related PQ difficulties, correct the power factor, and is well suited for coordinative operation and control with RESs uncertainty. The position, size, and dynamic VAr control of UPQC, on the other hand, are key influencing variables for enhancing the performance and PQ of electrical distribution systems (EDSs). This paper describes an upgraded UPQC configuration known as open-UPQC (UPQC-O) for reducing PQ difficulties caused by the inclusion of PVs and EVs. Further, an efficient gazelle optimization algorithm (GOA) is suggested to solve the multi-objective optimal allocation of the PV-UPQC-O issue with an emphasis on voltage quality, distribution losses, and voltage stability. Simulations were performed for various scenarios using a modified IEEE 33-bus test system. According to the comparison data, the PV-UPQC-O improved the feeder performance more effectively than the standard UPQC and UPQC-O. The proposed PV-UPQC-O results for total loss reduction of 76.15% when compared to base case without EV load penetration. On the other hand, it is around 76.52% reduction when compared to base case with EV load penetration. Furthermore, the proposed GOA outperforms the prairie dog optimization (PDO), pelican optimization algorithm (POA) and coati optimization algorithm (COA) in terms of global solution and convergence.

Keywords: Power quality, Photovoltaic system, Electric vehicles, Unified power quality conditioner, Gazelle optimization algorithm, Multi-objective optimization.

1. Introduction

The global trend towards sustainability is focused on adaption of renewable energy sources (RESs) and electric vehicles (EVs) by aiming various techno, economic and environmental goals in energy sector and transportation sector, simultaneously. However, their randomness and uncertainty nature created various typical issues; particularly stability and power quality (PQ) based issues in electrical distribution system [1]. In [2], the effects of increasing photovoltaic (PV) and EV adoption on the power grid stability, power quality, and energy economics were examined. It begins with EV technologies and then discusses how the grid integration of EVs affects grid stability, power quality, and the energy market. The report also examined the effects of large-scale PV grid integration, including the PV structure and grid code requirements. Finally, grid integration of PV and EV has been shown to affect the electricity system operation. In [3], an in-depth examination of power quality mitigation in the context of solar PV integration into a utility grid was presented. They discuss renewable energy, solar energy integration, and power quality. The report covers problems related to the overall system network and proposes

strategies to address the PQ challenges associated with increased solar power penetration into the rural grid. It also includes IEEE standards for various PQ events, distribution flexible AC transmission system (DFACTS) device configurations, and control algorithms utilised for grid integration of PV systems. Unified power quality conditioner (UPQC) is one such effective device for handing PQ issues in electrical distribution systems (EDs). In [4], an exhaustive review of the different PQ devices including UPQC and its application in EDSs was presented by covering various topologies of PQ devices, compensation methods, control theories, and technological development.

However, the expected benefits of UPQC in EDSs may be realised only when they are optimally integrated and controlled in the system. Researchers have widely used various optimisation techniques, particularly meta-heuristic algorithms, to overcome the computing challenges in solving multi-objective optimisation problems using UPQC [5]. A case study on the use of a transformer-less UPQC to improve power quality in Cairo Airport's lighting system was presented in [6]. The proposed topology was optimised and empirically validated using an extended bald eagle search (EBES) optimizer. In [6], the JAYA optimisation algorithm was proposed to optimise the operation of the UPQC. The JAYA algorithm was utilised to find the optimal control parameters of the UPQC, resulting in improved utilisation of the device. In [7], beetle swarm-based butterfly optimisation (BS-BOA) was presented to optimise a multi-converter UPQC. This algorithm was utilised to determine the optimal control parameters of the UPQC, resulting in improved PQ in the system. In [8], a puzzle optimisation algorithm (POA) was employed to enhance the power quality in multi-microgrids by robustly controlling an adaptive power quality compensator. In [9], PSO-based sliding mode controller for UPQC VSCs was discussed. The PSO optimises the sliding mode controller parameters to improve the performance of the UPQC VSCs. In [10], an enhanced self-adaptive Bat Algorithm (BA) for optimising the location of the UPQC is introduced. The enhanced BA adaptively adjusts its parameters during the optimisation process, resulting in improved accuracy in determining the optimal location of the UPQC. In [11], Rao's algorithm was introduced to optimise the VA loading of the converter. This algorithm determines the optimal VA loading for the converter and maximises the utilisation of the UPQC. In [12], to mitigate harmonics and voltage instability in modern distribution power grids, Fixed Order Proportional-Integral (FOPI) controllers for static synchronous compensators (STATCOM) and unified power quality conditioners (UPQC) were proposed. The study applies the whale optimisation algorithm (WOA) to design FOPI controllers for STATCOM and UPQC. FOPI controllers mitigate harmonics and voltage instability and improve the power quality in modern distribution power grids. In [13], the performance of different control approaches for UPQC was compared using a heuristic approach. This study evaluates the performance of UPQC control systems based on proportional-integral (PI) grey wolf optimisation (GWO) (PI-GWO), fractional-order controllers, and a reinforcement learning agent, providing insights into their effectiveness in improving power quality. In [14], the artificial rabbit optimisation (ARO) algorithm was used for the optimal allocation of PV systems and passive power filters. The ARO algorithm determines the optimal locations and sizes of PV systems and power filters, leading to an enhanced power quality in the radial distribution network. In [15], an improved jellyfish algorithm (IJFA) for mitigating power quality issues in a PV integrated microgrid system was proposed. The IJFA optimises the control parameters of the microgrid system and improves the power quality performance. In [16], an investigation is presented to address the effectiveness of the UPQC in mitigating voltage sags, voltage swells, and harmonics caused by nonlinear loads. This study provides insights into the performance of UPQC under nonlinear load conditions. In [17], a PV-UPQC system controlled by a Neural Network was presented. The PV-UPQC integrates solar PV, battery energy storage, and power conditioning capabilities to improve power quality in grid-connected operations.

The literature describes UPQC research gaps as investigating alternative optimization methodologies to improve integration and control approaches in EDS [18]. Although meta-heuristic algorithms are often used, multi-objective UPQC optimization difficulties need testing several optimisation methods [19]. Therefore, this research provides an optimization strategy to reduce PQ issues produced by RESs and EVs. Gazelle optimization algorithm (GOA) [20] can handle the multi-objective optimum PV-UPQC-O allocation problem with an emphasis on voltage quality, distribution losses, and voltage stability.

The following are the major contributions of this study.

1) To improve the overall performance of EDS under EV penetration by optimally integrating hybrid PV-UPQC-O.

2) To analyse and improve the EDS performance with different configurations, namely, PV, PV-DSSSC, PV-UPQC-O$_1$ (single shunt VSC) and PV-UPQC-O$_3$ (three shunt VSCs).

3) To compare the effectiveness of PV, PV-DSSSC, PV-UPQC-O$_1$ and PV-UPQC-O$_3$ without and with EV penetrations.

4) Further, to introduce gazelle optimization algorithm (GOA) for the first time to solve PV allocation problem in EDS considering power quality devices.

The paper's structure unfolds as follows: Section 2 details PV-UPQC-O and EV load modelling. Section 3 introduces a multi-objective optimization problem with equal and unequal constraints. Section 4 delves into the GOA solution approach. Section 5 showcases IEEE 33-bus simulation results across various scenarios. Lastly, Section 6 summarizes key research findings comprehensively.

2. Modelling of theoretical concepts

This section explains the mathematical modelling of PV penetration and hourly network loading profile are explained. Two voltage-sourced VSCs, a series inverter and shunt inverter, make up the UPQC-O [21]. In a healthy network, the series inverter is intended to support VAr, and in a voltage sag scenario, it is intended to reduce the supply voltage sag. Conversely, shunt VSCs are designed to remove line-current harmonics and offer VAr support to a network. It is thought that a sample radial distribution network, as shown in Fig. 1, represents the steady-state model of PV-UPQC-O [22].

2.1 PV-UPQC-O

The DC power generation from a PV system can be injected into main grid via a shunt/ series DC/AC converter/ voltage source converter (VSCs). Thus, as shown in Fig. 1, the series VSCs of UPQC-O is used for the same purpose.

With this configuration, branch-*sr* can be seen as equivalent to PV system embedded with distribution static synchronous series compensator (PV-DSSSC) and its steady-state power injections given by [23]:

$$P_{s(inj)} = -V_sV_{se}\left\{g_{sr}cos(\theta_{s,se}) + \left(b_{sr} + \frac{b_c}{2}\right)sin(\theta_{s,se})\right\} \quad (1)$$

$$Q_{s(inj)} = -V_sV_{se}\left\{g_{sr}sin(\theta_{s,se}) - \left(b_{sr} + \frac{b_c}{2}\right)cos(\theta_{s,se})\right\} \quad (2)$$

$$P_{r(inj)} = V_rV_{se}\{g_{sr}cos(\theta_{s,se}) + b_{sr}sin(\theta_{r,se})\} \quad (3)$$

$$Q_{r(inj)} = V_rV_{se}\{g_{sr}sin(\theta_{s,se}) - b_{sr}sin(\theta_{r,se})\} \quad (4)$$

where V_s, V_r and V_{sr} are the voltage magnitudes of bus-*s*, bus-*r* and series voltage source, respectively; θ_s, θ_r and θ_{sr} are the voltage phase angles of bus-*s*, bus-*r* and series voltage source, respectively; $\theta_{s,se} = (\theta_s - \theta_{se})$ and $\theta_{r,se} = (\theta_r - \theta_{se})$, $y_{sr} = (g_{sr} + jb_{sr})$ is the admittance of branch-*sr*, $\frac{b_c}{2}$ is the half-line charging admittance, $P_{s(inj)}$ and $Q_{s(inj)}$ are the real and reactive power injections at bus-*s*, respectively; , $P_{r(inj)}$ and $Q_{r(inj)}$ are the real and reactive power injections at bus-*r*, respectively.

The net effective real and reactive power loadings at bus-*s* due to real and reactive power injections by PV-DSSSC and reactive power injections nu shunt VSCs are given by:

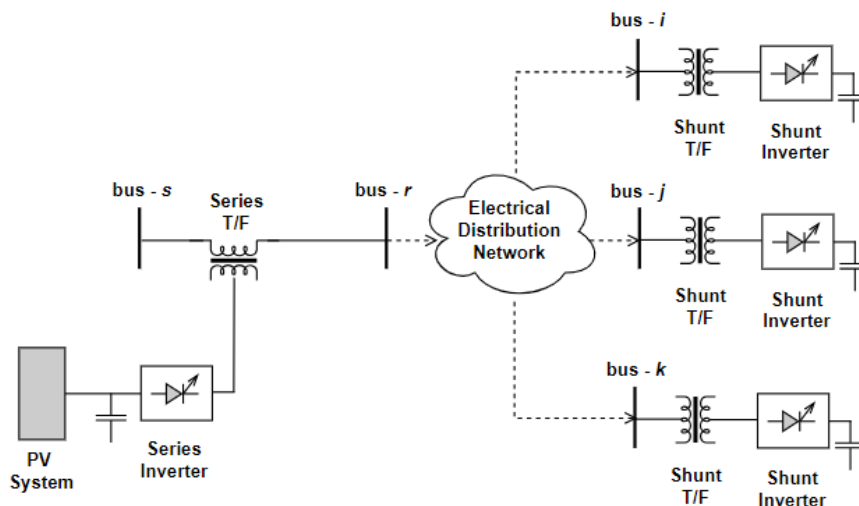$$\bar{P}_{d(s)} = P_{d(s)} - P_{pv(s)} - P_{s(inj)} \quad (5)$$

Figure. 1 A sample distribution feeder with schematic of PV-UPQC-O with multiple shunt VSCs

$$\bar{Q}_{d(s)} = Q_{d(s)} - Q_{s(inj)} \qquad (6)$$

$$\bar{P}_{d(r)} = P_{d(r)} - P_{r(inj)} \qquad (7)$$

$$\bar{Q}_{d(r)} = Q_{d(r)} - Q_{r(inj)} \qquad (8)$$

In order to formulate PV-UPQC-O configuration, shunt inverters/ VSCs need to be integrated either at single location or multiple locations.

$$\bar{Q}_{d(m)} = Q_{d(m)} - Q_{o(inj),m}, \quad \forall m = i, j, k \qquad (9)$$

where $\bar{P}_{d(s)}$ and $\bar{Q}_{d(s)}$ are the real and reactive power loads of bus-s after integrating PV-DSSSC, respectively; where $\bar{P}_{d(r)}$ and $\bar{Q}_{d(r)}$ are the real and reactive power loads of bus-r after integrating PV-DSSSC, respectively; $P_{d(s)}$ and $Q_{d(s)}$ are the base case real and reactive power loads of bus-s, respectively; ; $P_{d(r)}$ and $Q_{d(r)}$ are the base case real and reactive power loads of bus-r, respectively; $P_{pv(s)}$ is the real power injection by PV system at bus-s, $Q_{o(inj)}$ is the reactive power injections by shunt VSCs.

2.2 Modeling of EV load

Integration of EV load at a bus via AC/DC converter can cause for increment in both net effective real and reactive loadings and given by:

$$\bar{P}_{d(n)} = P_{d(n)} + P_{ev(n)}V_n^{\alpha_{ev}} \qquad (10)$$

$$\bar{Q}_{d(n)} = Q_{d(n)} + P_{ev(n)}tan(\theta_{ev})V_n^{\beta_{ev}} \qquad (11)$$

where $\bar{P}_{d(n)}$ and $\bar{Q}_{d(n)}$ are the real and reactive power loads of bus-n after integrating EV, respectively; $P_{d(n)}$ and $Q_{d(n)}$ are the base case real and reactive power loads of bus-n, respectively; $P_{ev(n)}$ is the real power load of EV at bus-p, θ_{ev} is the operating power factor EV charger, V_n is the voltage magnitude of bus-n, α_{ev} and β_{ev} are the exponents of real and reactive power loadings of EV load modelling [24].

3. Main title

This section explains the proposed multi-objective function focusing on real power loss reduction (P_{loss}), improvement in voltage quality index (VQI) and feeder loadability margin (LM)

enhancement. Further, it also explains various operational and planning constraints under study.

$$P_{loss} = \sum_{k=1}^{nbr} I_k^2 r_k \qquad (12)$$

$$VQI = \frac{1}{nb}\sqrt{\sum_{m=1}^{nb}(V_{ss} - V_m)^2} \qquad (13)$$

$$LM = \lambda_{max}\sum_{k=1}^{nb}\left[P_{d(k)} + jQ_{d(k)}\right] \qquad (14)$$

where nbr and nb are the number of branches and number of buses in the feeder, respectively; V_{ss} and V_m are the voltages of substation and bus-m, respectively; $P_{d(k)}$ and $Q_{d(k)}$ are the real and reactive power loading of bus-k, respectively; λ_{max} is the real scalar to express feeder loadability level, r_k and I_k are the resistance and current flow of branch-k, respectively.

The multi-objective function is formulated to minimize simultaneously these three objectives and is given by:

$$OF = P_{loss} + VQI + \frac{1}{LM} \qquad (15)$$

The following are the constraints considered while solving the multi-objective function.

$$P_{pv(p)} \leq (P_D + P_{loss}) \qquad (16)$$

$$\left[Q_{s(inj)} + Q_{r(inj)} + \sum_{m=1}^{nSh} Q_{o(inj),m}\right] \leq Q_D \qquad (17)$$

$$V_{ss} \leq V_m \leq V_{min} \qquad (18)$$

$$I_k \leq I_{k,max} \qquad (19)$$

Here, Eqs. (16) and (17) are used to limit the over compensation in the feeder due to PV and UPQC-O, respectively; Eqs. (18) and (19) are used to define limits for bus voltage magnitudes and branch currents, respectively.

In order to evaluate P_{loss} and VQI, NR load flow method is employed. Further, to determine LM, the load at all buses is increased simultaneously until NR method fails to converge. The amount of increased load from the base case loading is treated as loadability margin LM.

4. Gazelle optimization algorithm

This section explains the gazelle optimization algorithm (GOA) [28]. It mimics gazelles' survival tactics in a predator-driven habitat. It adapts their evasion strategies in an algorithmic framework to tackle real-world optimization, alternating between

peaceful grazing and evasive manoeuvres when predators are spotted for solution discovery.

The GOA employs a population-based approach, initializing search agents as gazelles (G) in a matrix form for solutions in Eq. (20). Their positions, governed by Eq. (21), are stochastically generated within defined bounds (l_b and u_b). Each candidate's vector, g_{ij} is randomly positioned in n gazelles across d dimensions in the optimization problem's search space.

$$G = \begin{bmatrix} g_{1,1} & \cdots & g_{1,d} \\ \vdots & \ddots & \vdots \\ g_{n,1} & \cdots & g_{n,d} \end{bmatrix} \tag{20}$$

$$g_{ij} = r(u_b - l_b) + l_b \tag{21}$$

Each iteration generates candidate solutions (g_{ij}). The best found becomes the elite gazelle (g'_{ij}), mirroring nature's adeptness in spotting, alerting others, and escaping predators. This elite forms a matrix as given in Eq. (22) guiding further gazelle steps.

$$E = \begin{bmatrix} g'_{1,1} & \cdots & g'_{1,d} \\ \vdots & \ddots & \vdots \\ g'_{n,1} & \cdots & g'_{n,d} \end{bmatrix} \tag{22}$$

In GOA, predators and gazelles act as search agents. When a predator is sighted, both flee towards safety, exploring the same direction. The elite updates if a superior gazelle replaces the top one at each iteration's end.

4.1 Exploitation phase

During this phase, the gazelles graze undisturbed either in the absence of a predator or while being observed by one. Here, their movement follows Brownian motion, marked by methodical and uniform steps, efficiently covering adjacent regions within their habitat. The mathematical representation of this behaviour is described in Eq. (23).

$$g_i^{k+1} = g_i^k + s_g \cdot r \cdot r_b \cdot \left(E_i - r_b \times g_i^k \right) \tag{23}$$

where g_i^{k+1} represents the solution in the upcoming iteration, while g_i^k stands for the current iteration's solution, s_g signifies the grazing speed of gazelles, and r_b is a vector of random values portraying Brownian motion, derived from vector r consisting of uniform random numbers [0,1].

4.2 Exploration phase

Upon spotting a predator, gazelles respond by tail flicking, foot stomping, or bounding up to 2 meters-scaled between 0 and 1. This behaviour, simulated by Lévy flight, involves small steps and occasional long jumps, enhancing searchability in optimization. Gazelles and predators abruptly change directions, alternating behaviour per iteration-gazelles using Lévy flight on odd iterations, predators initially employing Brownian motion before Lévy flight.

$$g_i^{k+1} = g_i^k + S_g \cdot \gamma \cdot r \cdot r_l \cdot \left(E_i - r_l \cdot g_i^k \right) \tag{24}$$

where S_g represents the maximum speed achievable by a gazelle, while r_l signifies a vector derived from random numbers following Lévy distributions, $\gamma = [1, -1]$. Eq. (25) illustrates the mathematical model governing the predator's behaviour in pursuit of the gazelle.

$$g_i^{k+1} = g_i^k + S_g \cdot \gamma \cdot \delta \cdot r_b \cdot \left(E_i - r_l \cdot g_i^k \right) \tag{25}$$

$$\delta = \left(1 - \frac{k}{k_{max}} \right)^{\left(\frac{2k}{k_{max}} \right)} \tag{26}$$

where δ is the cumulative effect of the predator. This factor represents the overall impact of the predator. In research on Mongolian Gazelles, despite their non-endangered status, they have a 0.66 annual survival rate, implying predators succeed only 0.34 times. Predator Success Rates (P), influence gazelles' escape ability, preventing the algorithm from getting stuck in local minima. Its modelled effect is detailed in Eq. (27).

For $r \leq P$

$$g_i^{k+1} = \{ g_i^k + \delta \cdot [r \cdot (u_b - l_b) + l_b] \cdot U \tag{27}$$

Otherwise,

$$g_i^{k+1} = [\{ g_i^k + P \cdot (1 - r) + r] \cdot \left(g_{r1}^k - g_{r2}^k \right) \tag{28}$$

where r is a random number between 0 and 1, g_{r1}^k and g_{r2}^k are randomly selected gazelles within the same iteration, respectively; U is a binary vector defined by Eq. (29).

$$U = \begin{cases} 0 & if \ r < 0.34 \\ 1 & else \end{cases} \tag{29}$$

In this ways, GOA's exploitation phase mirrors gazelles grazing undisturbed or while being stalked

by a predator. Once a predator is sighted, the algorithm shifts into the exploration phase, wherein gazelles evade the predator, reaching safety. These steps iterate until meeting termination criteria, seeking optimal solutions in optimization problems. Further, the computational features of GOA can be explored more in [20].

5. Simulation results

Simulation studies are performed on IEEE 33-bus distribution system for different scenarios. At fist scenario, the performance of feeder is improved by integrating PV system optimally in the network. In the second scenario, the maximum possible size of UPQC is evaluated at PV bus (shunt converter bus) to formulate PV-UPQC system. Finally, the optimal locations for series converter buses are determined along with proper sizes for formulating PV-UPQC-O configuration.

5.1 Without EV load penetration

Case 0: The base case test system has total constant power load of 3715 kW and 2300 kVAr and operates at 11 kV. By NR load flow, the distribution losses are evaluated as 210.9976 kW and 143.0325 kVAr, respectively. Further, the lowest voltage magnitude is determined as 0.9038 p.u. at bus-18.

Case 1: In this case, the optimal location and size of PV system is determined using proposed methodology. The search space boundary for locations is bus-2 to bus-33 and for the sizes, 0 to 3715 kW, respectively. By using GOA, the size of PV system is estimated as 2590.241 kW at bus-6. The distribution losses are reduced to 111.0298 kW and 81.6840 kVAr, respectively. Further, the lowest voltage magnitude is raised to 0.9424 p.u. at bus-18. The simulation results PV allocation using GOA and other methods are given in Table 1.
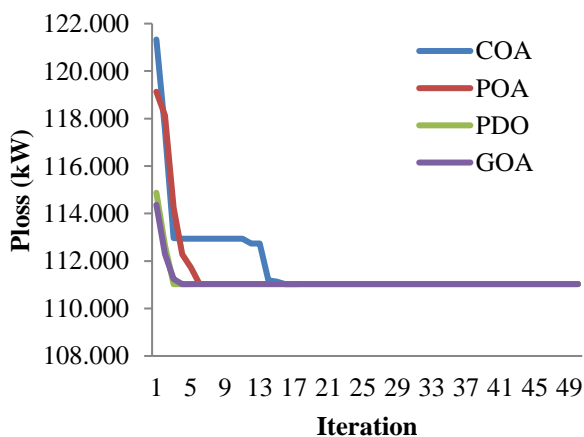
Table 1. Comparison of different algorithms

Item	COA	POA	PDO	GOA
PV_{size} (kW)	2590	2590	2590	2590
PV_{bus} (#)	6	6	6	6
P_{loss} (kW)	110.03	110.03	110.03	110.03
Q_{loss} (kVAr)	81.684	81.684	81.684	81.684
V_{min} (p.u.)	0.9424	0.9424	0.9424	0.9424
$V_{min,bus}$ (#)	18	18	18	18
Best	111.03	111.03	111.03	111.03
Worst	121.33	119.13	114.88	114.37
Mean	111.78	111.44	111.14	111.13
Median	111.03	111.03	111.03	111.03
SD	1.798	1.566	0.586	0.501
Time (sec)	32.341	31.316	30.167	30.018

Further to GOA, simulations are performed with prairie dog optimization (PDO) [25], pelican optimization algorithm (POA) [26] and coati optimization algorithm (COA) [27]. For all algorithms, the population size and the number of maximum iterations are considered as 30 and 50, respectively. The statistical analysis of 25 independent runs of each algorithm is given in Table 1. All algorithms are resulted for same global optima, however, GOA has shown superiority in terms of least mean and standard deviation. The convergence characteristics of compared algorithms are given in Fig. 2. As can be observed, GOA has avoided sliding into the local optima trap and has attained global optima while maintaining consistent search features.

5.2 Comparative Study with Literature

A comparative study with literature works performed using pathfinder algorithm (PFA) [28], mayfly optimization algorithm (MOA) [29] and coyote optimization algorithm (COA) [30], as given in Table 2. For all algorithms, the size of PV system is estimated as 2590.241 kW at bus-6. The distribution losses are reduced to 111.0298 kW and 81.6840 kVAr, respectively. Further, the lowest voltage magnitude is raised to 0.9424 p.u. at bus-18. From this, it is very clear that GOA can be said that a competitive algorithm to literature works.

Case 2: In this case, the optimal location and size of PV system along with DSSSC parameters are determined.

Figure. 2 Convergence characteristics

Table 2. Comparison of different algorithms

Reference	PV_{size} (kW)/ bus	P_{loss} (kW)
PFA [28]	2590.264/ 6	111.03
MOA [29]	2590.264/ 6	111.03
COA [30]	2590/ 6	111.03
GOA	2590.264/ 6	111.03

Table 3. Comparison of different configurations without EV load penetration

Case	Configuration	PV (kW)/ bus	Series	Shunt	P_{loss} (kW)	Q_{loss} (kVAr)	V_{min} (p.u.)
0	Base		—	—	210.998	143.033	0.9038 (18)
1	PV	2590.24(6)	—	—	111.0298	81.684	0.9424 (18)
2	PV-DSSSC	2558.51(6)	1761.35(6)	—	67.8685	54.8324	0.9583 (18)
3	PV-UPQC-O_1	2558.51(6)	1747.01(6)	335.08(30)	67.691	54.732	0.9583 (18)
4	PV-UPQC-O_3	2525.83(6)	733.61(6)	236.96(19) 370.08(25) 894.14(30)	50.3229	41.7397	0.9578 (18)

Table 4. Comparison of different configurations with EV load penetration

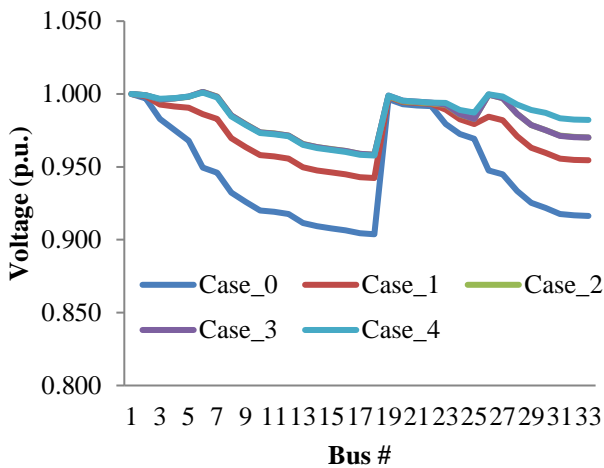| Case	Configuration	PV (kW)/ bus	Series	Shunt	P_{loss} (kW)	Q_{loss} (kVAr)	V_{min} (p.u.)
0	Base		—	—	314.647	213.139	0.9038 (18)
1	PV	3166.7(6)	—	—	161.3860	118.8062	0.9311 (18)
2	PV-DSSSC	3119.87(6)	2111.14(6)	—	98.9005	79.8620	0.9504 (18)
3	PV-UPQC-O_1	3075.42(6)	1023.29(6)	1056.91(19)	77.7105	63.8449	0.9499 (18)
4	PV-UPQC-O_3	3073.28(6)	866.01(6)	294.58(19) 453.10(25) 1056.96(30)	73.8733	61.1884	0.9496 (18)

Figure. 3 Comparison of voltage profile without EV load penetration at different case studies

At bus-6, the optimal PV and VSC of DSSSC sizes are to be 2558.51 kW and 1761.35 kVAr, respectively. By this, the losses are reduced to 67.8685 kW and 54.8324 kVAr, respectively. And, the minimum voltage is observed at bus-18 as 0.9583 p.u.

Case 3: In this case, the optimal location and size of PV system along with UPQC parameters with one series and one shunt VSCs are determined. At bus-6, the optimal PV and VSC of DSSSC sizes are to be 2558.51 kW and 1747.01 kVAr, respectively. And, the shunt VSC is determined at bus-19 as 335.08 kVAr. By this, the losses are reduced to 67.691 kW and 54.732 kVAr, respectively. And, the minimum voltage is observed at bus-18 as 0.9583 p.u.

Case 4: In this case, the optimal location and size of PV system along with UPQC parameters with one

series and three shunt VSCs are determined. At bus-6, the optimal PV and VSC of DSSSC sizes are to be 2525.83 kW and 733.608 kVAr, respectively. And, the shunt VSCs are determined at buses 19, 25 and 30 as 236.961 kVAr, 370.078 kVAr, and 894.136 kVAr, respectively. By this, the losses are reduced to 50.3229 kW and 41.7397 kVAr, respectively. And, the minimum voltage is observed at bus-18 as 0.9578 p.u.

In comparison to all case studies reported in Table 3, the PV-UPQC-O_3 allocation reduced the total losses and improved the voltage profile significantly. Further, the voltage profiles are given in Fig. 3.

5.3 With EV load penetration

Case 0: In this case, 25% extra load at all buses is considered as EV load penetration. Thus, the base case test system has total constant power load of 4526.02 kW and 2755.35 kVAr and operates at 11 kV. By NR load flow, the distribution losses are evaluated as 314.6476 kW and 213.1387 kVAr, respectively. Further, the lowest voltage magnitude is determined as 0.8827 p.u. at bus-18.

Case 1: In this case, the optimal location and size of PV system is determined using proposed methodology. By using GOA, the size of PV system is estimated as 3166.7 kW at bus-6. The distribution losses are reduced to 161.386 kW and 118.806 kVAr, respectively. Further, the lowest voltage magnitude is raised to 0.9311 p.u. at bus-18.

Case 2: In this case, the optimal location and size of PV system along with DSSSC parameters are determined. At bus-6, the optimal PV and VSC of DSSSC sizes are to be 3119.87 kW and 2111.14

kVAr, respectively. By this, the losses are reduced to 98.9 kW and 79.862 kVAr, respectively. And, the minimum voltage is observed at bus-18 as 0.9504 p.u.

Case 3: In this case, the optimal location and size of PV system along with UPQC parameters with one series and one shunt VSCs are determined. At bus-6, the optimal PV and VSC of DSSSC sizes are to be 3075.42 kW and 1023.29 kVAr, respectively. And, the shunt VSC is determined at bus-30 as 1056.91 kVAr. By this, the losses are reduced to 77.7105 kW and 63.8449 kVAr, respectively. And, the minimum voltage is observed at bus-18 as 0.9499 p.u.

Case 4: In this case, the optimal location and size of PV system along with UPQC parameters with one series and three shunt VSCs are determined. At bus-6, the optimal PV and VSC of DSSSC sizes are to be 3073.28 kW and 866.01 kVAr, respectively. And, the shunt VSCs are determined at buses 19, 25 and 30 294.58 kVAr, 453.1 kVAr, and 1056.96 kVAr, respectively. By this, the losses are reduced to 73.8733 kW and 61.1884 kVAr, respectively. And, the minimum voltage is observed at bus-18 as 0.9496 p.u.

In comparison to the base case without EV penetration, the losses with PV, PV-DSSSC, PV-UPQC-O_1, and PV-UPQC-O_3 are reduced by 47.38%, 67.83%, 67.92%, and 76.15%, respectively. However, the losses are increased by 49.12% (i.e., from 211 kW to 314.647 kW) with EV penetration, and they are again reduced significantly with PV, PV-DSSSC, PV-UPQC-O_1, and PV-UPQC-O_3 by 48.71%, 68.57%, 75.30%, and 76.52%, respectively. This indicates the need for hybridization of RESs with PQ devices, considering emerging load trends in modern EDSs.

6. Conclusion

The unified power quality conditioner (UPQC) stands out among PQ devices, addressing voltage issues, correcting power factors, and aligning with uncertain RESs. UPQC's positioning, sizing, and dynamic control significantly impact electrical distribution systems' (EDS) performance and PQ. This paper presents an upgraded UPQC, UPQC-O, easing PQ challenges from PVs and EVs. Using the gazelle optimization algorithm (GOA), it optimally allocates PV-UPQC-O, prioritizing voltage quality, losses, and stability. Simulations on an IEEE 33-bus system highlight PV-UPQC-O's superiority over standard UPQC and UPQC-O, while GOA surpasses PDO, POA, and COA in global solutions and convergence. However, it is further essential to analyze the computational efficiency of GOA, and the performance of the proposed hybrid system, i.e.,
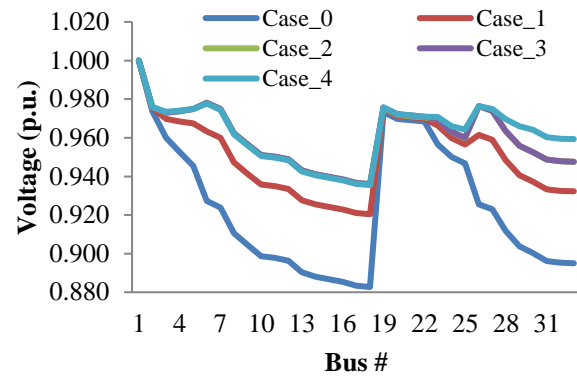

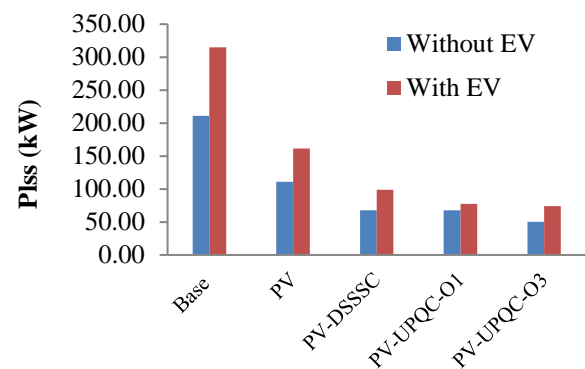Figure. 4 Comparison of voltage profile with EV load penetration at different case studies

Figure. 5 Comparison of P_{loss} without and with EV load penetration at different case studies
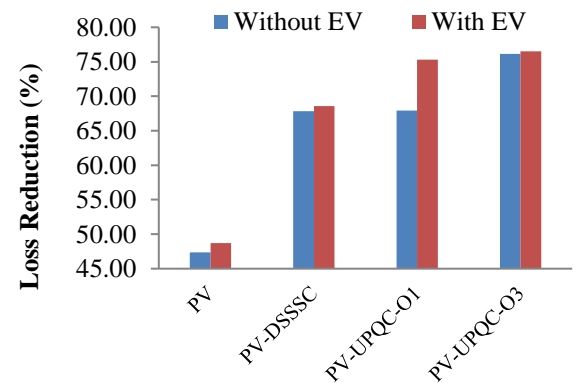

Figure. 6 Comparison of P_{loss} reduction without and with EV load penetration at different case studies

PV-UPQC-O, in larger networks needs to be investigated, which is treated as the future scope of this work.

Conflicts of Interest

The authors declare no conflict of interest.

Author Contributions

References

[1] A. Jenn and J. Highleyman, "Distribution grid impacts of electric vehicles: A California case study", *Energy Sources, Part A: Recovery, Utilization, and Environmental Effects*, Vol. 25, No. 1, 103686, 2022.

[2] P. Barman, L. Dutta, S. Bordoloi, A. Kalita, P. Buragohain, S. Bharali, and B. Azzopardi, "Renewable energy integration with electric vehicle technology: A review of the existing smart charging approaches", *Renewable and Sustainable Energy Reviews*, Vol. 183, pp. 113518, 2023.

[3] K. Jha and A. G. Shaik, "A comprehensive review of power quality mitigation in the scenario of solar PV integration into utility grid", *e-Prime-Advances in Electrical Engineering, Electronics and Energy*, 100103, 2023.

[4] S. Choudhury, G. K. Sahoo, "A Critical Analysis of Different Power Quality Improvement Techniques in Microgrid", *e-Prime-Advances in Electrical Engineering, Electronics and Energy*, 100520, 2024.

[5] E. Hernández-Mayoral, M. Madrigal-Martínez, J. D. Mina-Antonio, R. Iracheta-Cortez, J.A. Enríquez-Santiago, O. Rodríguez-Rivera, G. Martínez-Reyes, and E. Mendoza-Santos, "A Comprehensive Review on Power-Quality Issues, Optimization Techniques, and Control Strategies of Microgrid Based on Renewable Energy Sources", *Sustainability*, Vol. 15, No. 12, 9847, 2023.

[6] S. E. Abdel Mohsen, A. M. Ibrahim, Z. S. Elbarbary, and A.I. Omar, "Unified Power Quality Conditioner Using Recent Optimization Technique: A Case Study in Cairo Airport, Egypt", *Sustainability*, Vol. 15, No. 4, 3710, 2023.

[7] S. Gade and R. Agrawal, "Optimal utilization of unified power quality conditioner using the JAYA optimization algorithm", *Engineering Optimization*, Vol. 55, No. 1, pp. 1-8, 2023.

[8] J. I. Sankar and S. Subbaraman, "Multi-Converter UPQC Optimization for Power Quality Improvement Using Beetle Swarm-Based Butterfly Optimization Algorithm", *Electric Power Components and Systems*, pp. 1-2, 2023.

[9] H. F. Sindi, S. Alghamdi, M. Rawa, A. I. Omar, and A. H. Elmetwaly, "Robust control of adaptive power quality compensator in Multi-Microgrids for power quality enhancement using puzzle optimization algorithm", *Ain Shams Engineering Journal*, Vol. 14, No. 8, pp. 102047, 2023.

[10] M. A. Heidari, M. Nafar, and T. Niknam, "Particle Swarm Optimization Based Sliding Mode Controller for Performance Improvement of Unified Power Quality Controllers VSCs", *Journal of Southern Communication Engineering*, Vol. 12, No. 46, pp. 59-76, 2023.

[11] S. Gade and R. Agrawal, "VA Loading Optimization of a Converter Using the Rao Algorithm for Maximum Utilization of the Unified Power Quality Conditioner", *ECTI Transactions on Electrical Engineering, Electronics, and Communications*, Vol. 21, No. 1, pp. 248573-, 2023.

[12] M. M. Mahmoud, B. S. Atia, Y. M. Esmail, S. A. Ardjoun, N. Anwer, A.I. Omar, F. Alsaif, S. Alsulamy, and S.A. Mohamed, "Application of Whale Optimization Algorithm Based FOPI Controllers for STATCOM and UPQC to Mitigate Harmonics and Voltage Instability in Modern Distribution Power Grids", *Axioms*, Vol. 12, No. 5, pp. 420, 2023.

[13] M. Nicola, C.I. Nicola, D. Sacerdoțianu, and A. Vintilă, "Comparative performance of UPQC control system based on PI-GWO, fractional order controllers, and reinforcement learning agent", *Electronics*, Vol. 12, No. 3, pp. 494, 2023.

[14] C. R. Rao, R. Balamurugan, and R. K. Alla, "Artificial Rabbits Optimization Based Optimal Allocation of Solar Photovoltaic Systems and Passive Power Filters in Radial Distribution Network for Power Quality Improvement", *International Journal of Intelligent Engineering & Systems*, Vol. 16, No. 1, 2023, doi: 10.22266/ijies2023.0228.09.

[15] S. Suman, D. Chatterjee, and R. Mohanty, "A Novel Approach for Mitigating Power Quality Issues in a PV Integrated Microgrid System Using an Improved Jelly Fish Algorithm", *Journal of Bionic Engineering*, Vol. 20, No. 1, pp. 30-46, 2023.

[16] P. Bhardwaj, A. Verma, S. P. Jaiswal, S. Lata, "Synchronized Control Strategy of UPQC to Mitigate the Sag and Swell of Voltage", *Macromolecular Symposia*, Vol. 407, No. 1, 2200059, 2023.

[17] O. E. Okwako, Z.H. Lin, M. Xin, K. Premkumar, and A.J. Rodgers, "Neural Network Controlled

Solar PV Battery Powered Unified Power Quality Conditioner for Grid Connected Operation", *Energies*, Vol. 15, No. 18, pp. 6825, 2022.

[18] A. Heenkenda, A. Elsanabary, M. Seyedmahmoudian, S. Mekhilef, A. Stojcevski, and N.F. Ab Aziz, "Unified Power Quality Conditioners Based Different Structural Arrangements: A Comprehensive Review", *IEEE Access*, 2023.

[19] G. Schurz and P. Thorn, "Escaping the no free lunch theorem: a priori advantages of regret-based meta-induction", *Journal of Experimental & Theoretical Artificial Intelligence*, Vol. 36, No. 1, pp. 87-119, 2024.

[20] J. O. Agushaka, A.E. Ezugwu, and L. Abualigah, "Gazelle optimization algorithm: a novel nature-inspired metaheuristic optimizer", *Neural Computing and Applications*, Vol. 35, No. 5, pp. 4099-4131, 2023.

[21] S. Lakshmi and S. Ganguly, "An on-line operational optimization approach for open unified power quality conditioner for energy loss minimization of distribution networks", *IEEE Transactions on Power Systems,* Vol. 34, No. 6, pp. 4784-4795, 2019.

[22] S. K. Dash and P. K. Ray, "A new PV-open-UPQC configuration for voltage sensitive loads utilizing novel adaptive controllers", *IEEE Transactions on Industrial Informatics*, Vol. 17, No. 1, pp. 421-429, 2020.

[23] Y. Chen, D. Wang, J. Li, H. Fan, J. Li, Y. Luo, and L. Li, "A SSSC optimal configuration method to enhance available transfer capability considering multi-wind farm access", *IET Renew. Power Gener.*, Vol. 17, pp. 3777-3792, 2023.

[24] V. Janamala, K. Radha Rani, P. Sobha Rani, A. N. Venkateswarlu, S. R. Inkollu, "Optimal switching operations of soft open points in active distribution network for handling variable penetration of photovoltaic and electric vehicles using artificial rabbits optimization", *Process Integration and Optimization for Sustainability*, Vol. 7, No. 1, pp: 419-437, 2023.

[25] A. E. Ezugwu, J. O. Agushaka, L. Abualigah, S. Mirjalili, and A.H. Gandomi, "Prairie dog optimization algorithm", *Neural Computing and Applications*, Vol. 34, No. 22, pp. 20017-20065, 2022.

[26] P. Trojovský and M. Dehghani, "Pelican optimization algorithm: A novel nature-inspired algorithm for engineering applications", *Sensors*, Vol. 22, No. 3, pp. 855, 2022.

[27] M. Dehghani, Z. Montazeri, E. Trojovská, and P. Trojovský, "Coati Optimization Algorithm: A new bio-inspired metaheuristic algorithm for solving optimization problems", *Knowledge-Based Systems*, Vol. 259, pp. 110011, 2023.

[28] V. Janamala, "A new meta-heuristic pathfinder algorithm for solving optimal allocation of solar photovoltaic system in multi-lateral distribution system for improving resilience", *SN Applied Sciences*, Vol. 3, No. 1, pp. 118, 2021.

[29] M. S. Giridhar, K. R. Rani, P. S. Rani, and V. Janamala, "Mayfly Algorithm for Optimal Integration of Hybrid Photovoltaic/Battery Energy Storage/D-STATCOM System for Islanding Operation", *International Journal of Intelligent Engineering & Systems*, Vol. 15, No. 3, 2022, doi: 10.22266/ijies2022.0630.19.

[30] V. Janamala and D. S. Reddy, "Coyote optimization algorithm for optimal allocation of interline-Photovoltaic battery storage system in islanded electrical distribution network considering EV load penetration", *Journal of Energy Storage*, Vol. 41, pp. 102981, 2021.